Bulletin of the Seismological Society of America, Vol. 95, No. 2, pp. 502–511, April 2005, doi: 10.1785/0120000296

Rayleigh-Wave Group-Velocity Studies beneath the Indian Ocean

by D. D. Singh

Abstract The fundamental mode Rayleigh wave generated by 16 earthquakes, which occurred in the Indian Ocean and were recorded at 14 seismic stations of Asia, Africa, and Australia, are analyzed to estimate the Rayleigh-wave group velocity at periods of 10 to 60 sec by using the multiple filter analysis technique. In addition to this, Rayleigh-wave group-velocity data available in the literature across different propagation paths of the Indian Ocean forming a dense distribution of seismic wave traverses have been considered for tomographic studies. The group-velocity distribution maps have been obtained at periods of 10, 20, 30, 40, 50, and 60 sec for the Rayleigh wave. The minimum value of the group velocity of 2.0 km/sec is centered near the Rodriguez triple junction (25° S, 70° E) at 10 sec and higher value (3.4–4.0 km/sec) at 20 sec and greater period. As we move in the north-northwest direction from the Rodriguez triple junction, the Rayleigh-wave group-velocity isolines at 10 and 20 sec are also increasing in the northern direction in both the east and west sides of the ridge axis. Another minimum value of group-velocity isolines (1.9 km/sec) is centered near (25° S, 90° E) at 10 sec, and there is a gradual increase in the northern direction across the Ninetyeast Ridge. These observations are in accordance with the increase in the age of the ocean floor and there is a gradual increase in the group-velocity isolines. This can be interpreted as due to the hot uprising convection current, the material shows low shear-wave velocity along the ridge axis, and farther away from the ridge axis the material has become cooler with higher shear-wave velocity.

The inversion of Rayleigh-wave group-velocity across the Ninetyeast Ridge shows 120-km-thick LVZ (low-velocity zone) of shear-wave velocity of 4.38–4.78 km/sec at a depth of 40 km from the water surface, whereas other parts of the Indian Ocean show 44-km-thick LVZ with shear-wave velocity of 4.12–4.17 km/sec at a depth of 40 km from the water surface. The high shear-wave velocity below Moho (4.19–4.75 km/sec) beneath the Ninetyeast Ridge indicates the presence of a cold and dense lithosphere beneath it.

Introduction

The Indian Ocean is one of the largest oceans in the world, and the tectonic processes for the evolution of this ocean are more complex in nature than most others. The seismic wave velocity beneath the Indian Ocean will help in solving the complexities of the tectonic processes for its evolution. In recent years, several surface-wave tomographic studies have been made to understand the evolution of the Indian Ocean (Lana and Carbonell, 1987; Montagner, 1986; Montagner and Jobert, 1988; Patnaik and Mitchell, 1984). Additionally, surface-wave dispersion studies across different propagation paths of the Indian Ocean have been made by several researchers (Brune and Singh, 1986; Roult *et al.*, 1987; Souriau, 1981; Singh, 1988a,b). In most tomographic studies, longer periods (greater than 50 sec) of fundamental mode surface waves have been selected to provide deeper structure. In this study, we have estimated the fundamental mode Rayleigh-wave group velocity at the shorter period (10 to 60 sec) using the multiple filter analysis technique for various propagation paths of the Indian Ocean (Fig. 1). For this purpose, we have selected 16 earthquakes, which occurred in the Indian Ocean and were recorded at 14 WWSSN stations of Asia, Africa, and Australia (Fig. 1 and Table 1). Additionally, we have included all the propagation paths of the Indian Ocean given by Brune and Singh (1986), Singh (1988a,b), and Souriau (1981). These studies will help to increase our understanding of the tectonics and the origin of the Indian Ocean by using Rayleigh-wave tomographic and shear-wave velocity structure studies.

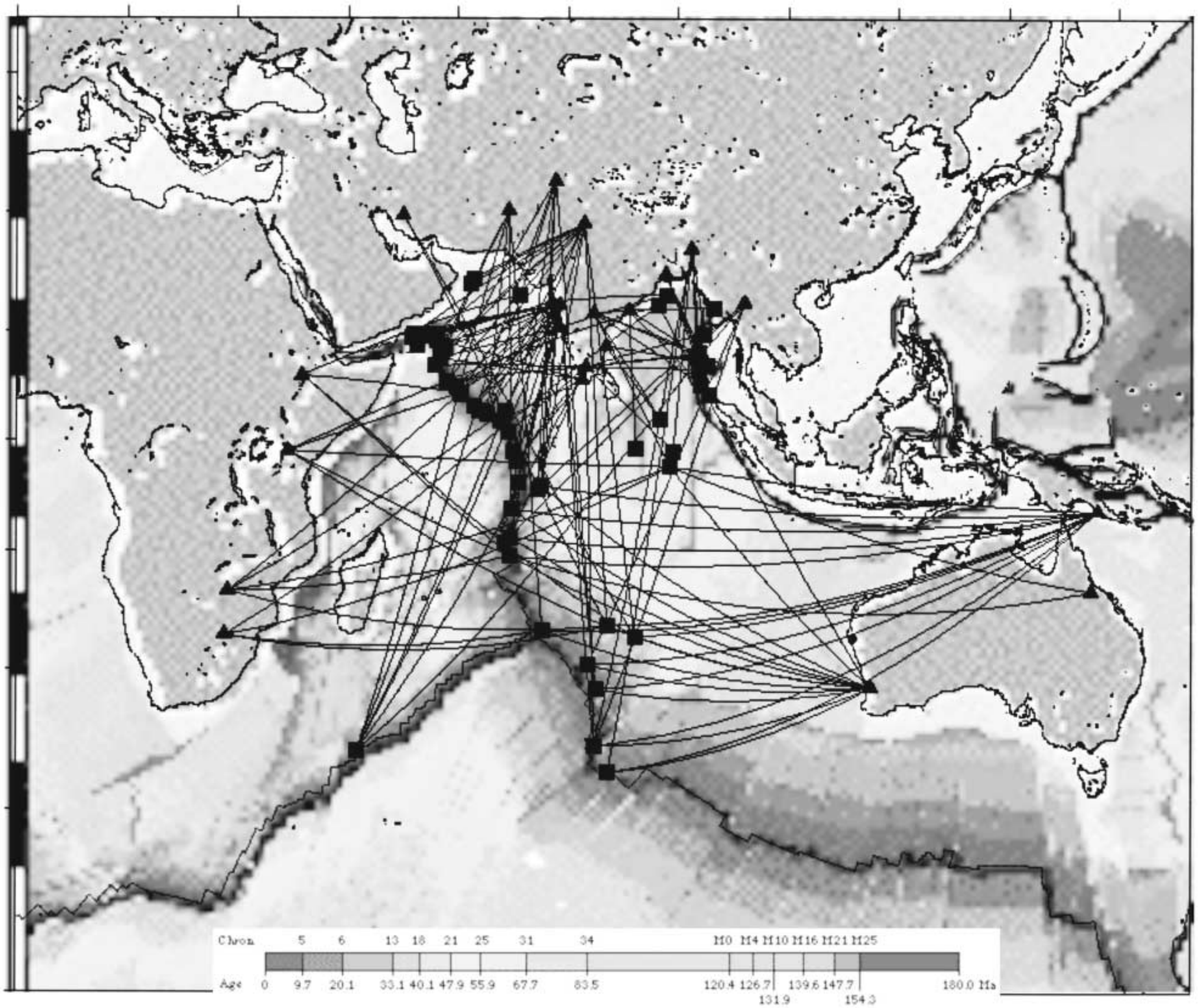

Figure 1. Earthquake epicenters (square) and seismic stations (triangle) are shown for the surface-wave tomography studies for more than 100 propagation paths of the Indian Ocean. Digital isochrones of the Indian Ocean floor have been taken from the Web site of Prof. R. D. Muller (www.geosci.usyd.edu.au).

Data Analysis

The details of the earthquake parameters for the surface-wave tomographic studies are listed in Table 1. The earthquake parameters have been taken from the International Seismological Centre Bulletins. Figure 1 shows the epicenter of 16 earthquakes and 14 seismic stations used in the study. The vertical component record is used for the Rayleigh wave. The Rayleigh-wave records are digitized at irregular intervals and then interpolated at fixed periods of 0.1 sec (time interval) by using the Lagrangian interpolation method. The digitized and interpolated data are detrended to remove the average and linear trends. The instrumental correction is applied using the relation given by Teng and Ben-Menahem (1965). The multiple filter analysis technique of Dziewonski *et al.* (1969) is used to estimate the fundamental mode Rayleigh-wave group velocity at periods of 10, 20, 30, 40, 50, and 60 sec. Figure 2 shows an example of the Rayleigh-wave group-velocity estimate by using the multiple filter analysis technique. Additionally, we have included the Rayleigh-wave group-velocity values given by Brune and Singh (1986), Singh (1988a,b), and Souriau (1981) to form a dense distribution of seismic wave propagation paths in the Indian Ocean. The total number of traverses varied at each period because of the different length of the trajectories, but it never fell below 60. The traces for all periods covered the areas uniformly and the propagation paths varied from 60 to 150 at periods of 10 to 60 sec.

Group-Velocity Tomography

The method used in the surface-wave tomography studies is based on the Backus and Gilbert formalism for the

Table 1
Earthquake Parameters Used in the Present Study for the Surface-Wave Tomography and Dispersion Studies

Station No.	Date	Origin Time (UTC)	Epicenter Latitude	Epicenter Longitude (° E)	Depth (km)	Magnitude M_b
1	18 Oct. 1967	16:23:25.8	25.1° S	71.5	19	5.7
2	27 Nov. 1967	10:46:48.6	13.0° S	67.1	33	5.2
3	14 Sep. 1967	01:25:19.1	24.5° S	80.4	3	5.5
4	6 June 1974	18:37:7.4	4.2° N	66.5	33	5.4
5	15 June 1974	3:32:48.1	13.7° N	50.5	65	5.2
6	26 Mar. 1975	16:19:19.7	19.8° N	68.4	24	5.2
7	28 Aug. 1975	18:25:44.1	25.9° S	84.2	33	5.4
8	3 Jan. 1977	6:15:50.	6.7° N	60.3	38	5.0
9	29 Jan. 1978	2:32:17.	15.5° S	67.2	33	5.1
10	17 Mar. 1979	6:32:29.7	3.0° S	68.1	20	5.4
11	8 Jul. 1979	4:09:10:	14.6° N	53.8	35	5.2
12	22 Jul. 1979	13:11:39.9	7.0° S	67.2	10	5.4
13	25 Dec 1979	23:46:33.5	2.7° S	68.0	4	5.3
14	28 Jan. 1980	14:46:39.3	3.4° S	88.9	33	5.4
15	13 May 1983	10:01:13.1	22.2° S	69.2	10	5.1
16	01 Jul. 1985	02:23:57.2	18.4° N	87.3	47	5.3

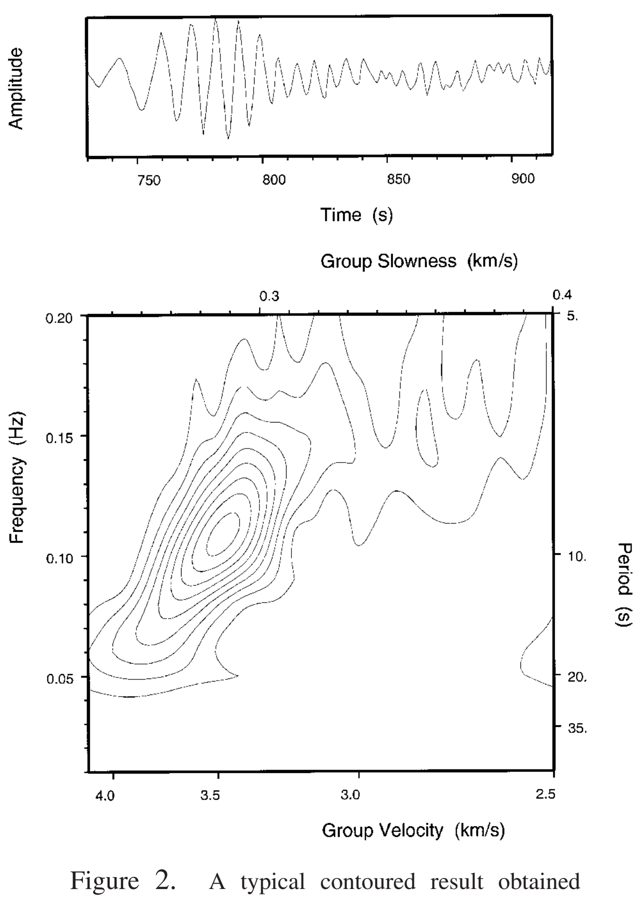

Figure 2. A typical contoured result obtained from multiple filter analysis of the vertical component event 8 (Table 1) recorded at New Delhi (NDI) seismic station (Dorman's package, personal communication).

linear inversion of travel times, extended for 2D and 3D inhomogeneous media (Yanovskaya, 1982; Gobarenko *et al.*, 1987; Wu and Levshin, 1994) and is intended for the estimation of the average velocity corrections relative to the starting velocity model from a finite set of travel times along the ray paths crossing the area under the investigation. The method is described in detail by Yanovskaya (1982), Gobarenko *et al.* (1987), and Wu and Levshin (1984). Velocity perturbation, smoothing radius, and precision accuracy are computed at the nodes that are 1° × 1° grid apart in a 45° × 45° grid covering an area of the Indian Ocean between latitudes 20° N and 25° S and longitudes of 50° E and 95° E. Calculations are made by using several smoothing parameters of 0.01, 0.05, 0.1, and 0.3. The smoothing parameter of 0.3 is selected in this study. The depth of penetration of surface waves increases with increasing period. The Rayleigh wave of 20-sec period gives approximately 20 km depth of penetration.

Figure 3 shows the group-velocity distribution maps at periods of 10, 20, 30, 40, 50, and 60 sec for the Rayleigh wave and the corresponding error estimates (mean square error) in Figure 4 and the error varies between 0.06 and 0.19 km/sec. At periods of 10 sec and 60 sec, the error is more (0.1 km/sec to 0.19 km/sec), but it is less than 0.12 km/sec at other periods, which is within the error limit of the accuracy. Figure 5 shows the distribution of the resolving radius. The area under the present investigation is roughly 4950 km × 4950 km. The distribution of the resolving radius lies between 2000 and 6000 km of the smoothing radius in most of the region, which is sufficient enough for getting the good resolution of the observed data (group velocity of Rayleigh wave) in the present study.

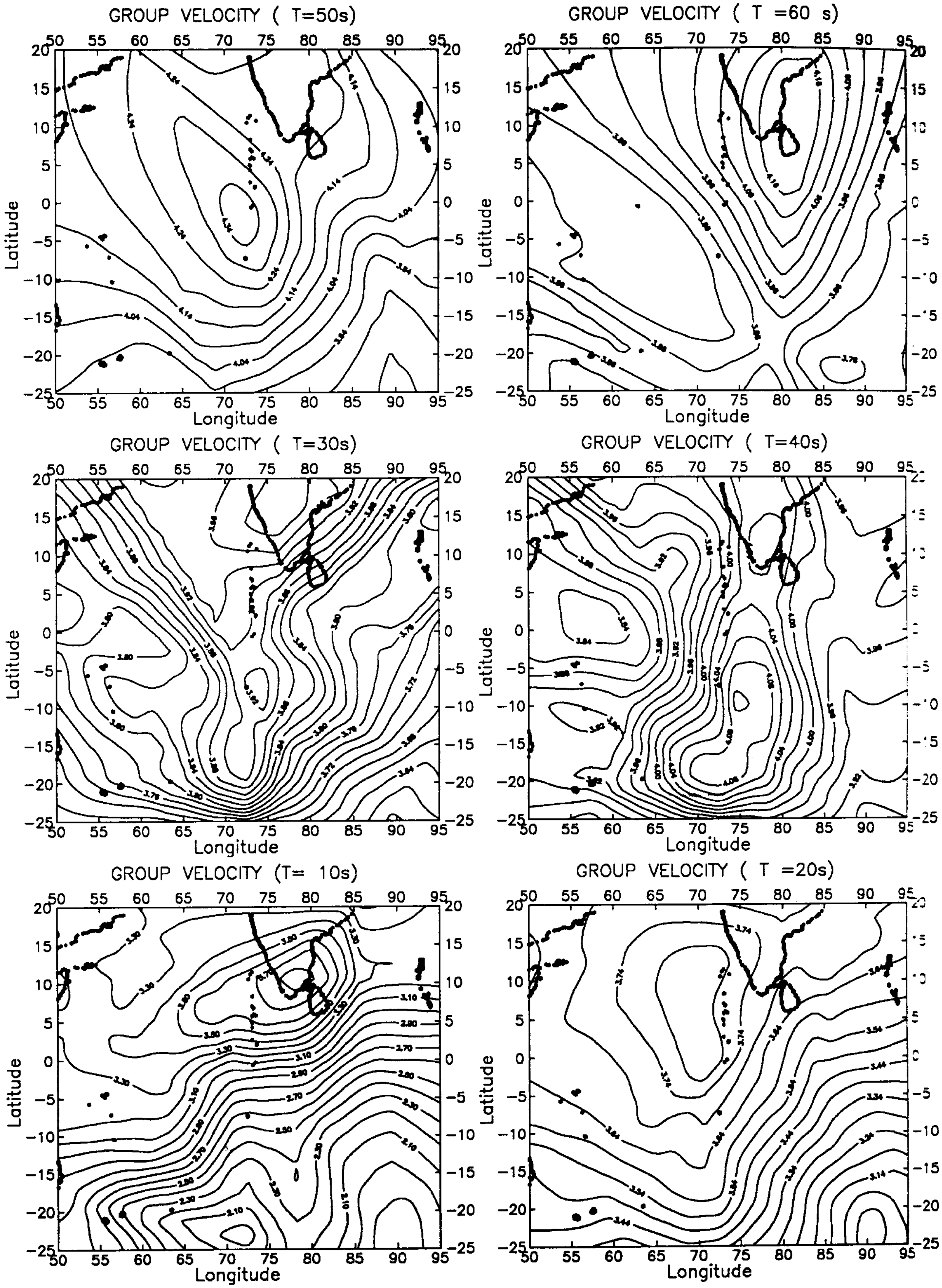

Figure 3. The pattern of lateral Rayleigh-wave group-velocity distribution resulting from the inversion at periods of 10, 20, 30, 40, 50, and 60 sec for the Indian Ocean. The continental boundary is shown by the dark symbol.

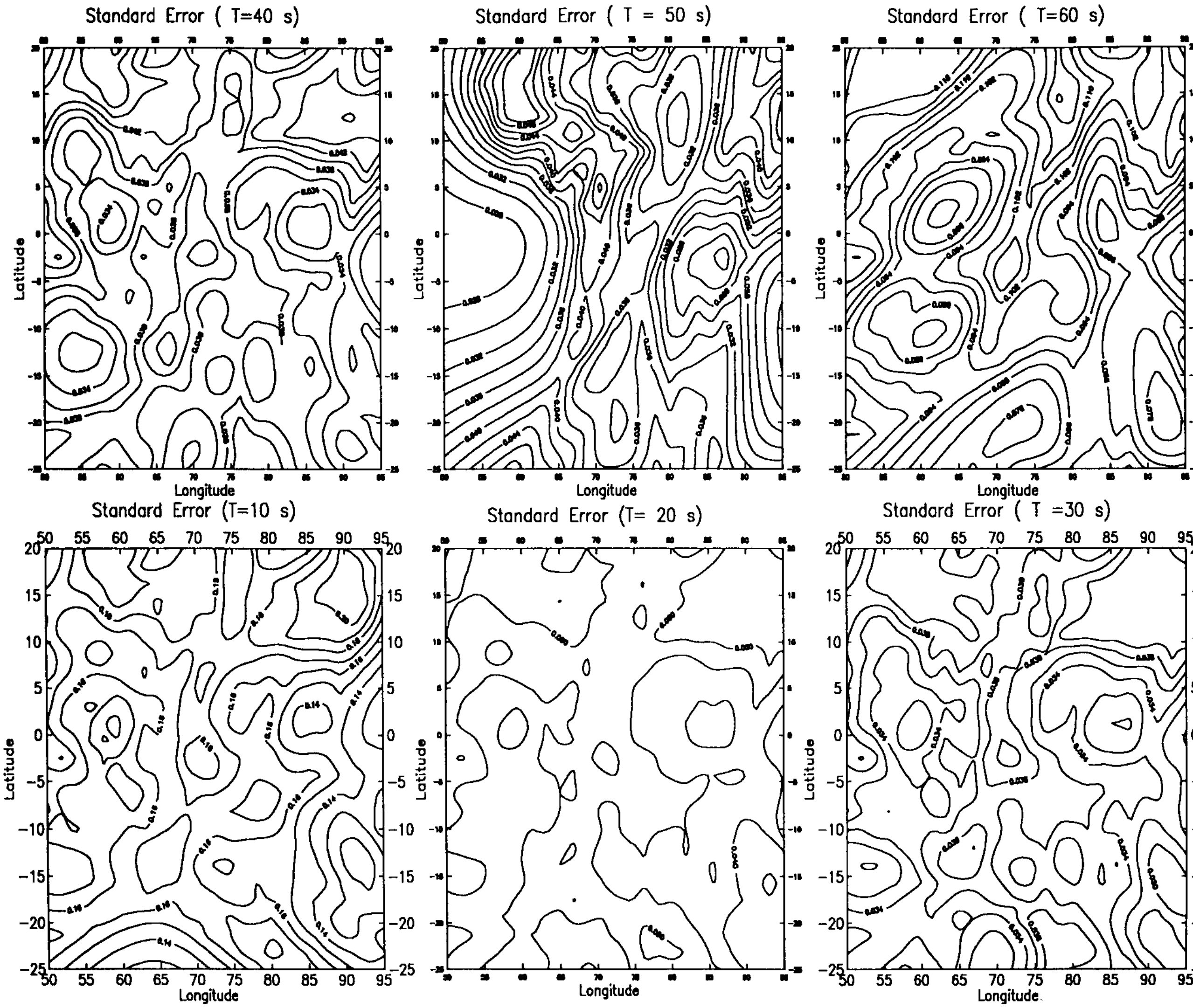

Figure 4. Rayleigh-wave group-velocity mean square errors in the Indian Ocean resulted from the inversion of the observed group-velocity data at the periods of 10, 20, 40, 50, and 60 sec.

Dispersion Analysis

Figure 1 shows the location of earthquakes and the seismic stations. The earthquake parameters are listed in Table 1. We selected earthquakes with good signal-to-noise ratio. These earthquakes are recorded on the seismic stations of Asia, Africa, and Australia. The vertical component is used for the Rayleigh wave. After the necessary filtering of the records between the frequency band of 0.01 and 0.1 Hz, the instrumental correction is applied to the data mentioned earlier. After getting the instrumentally corrected spectra, the multiple filter analysis is done to get the group velocity at the period of 10 to 60 sec with the Herrmann (1987) software package. The correction for the continental path is done (Brune and Singh, 1986).

We subdivided the study area into four different A, B, C, and D paths. Path A corresponds to the region lying between the spreading center and the Ninetyeast Ridge in the eastern side of the Indian Ocean. Path B is the region lying between spreading centers and the western side of the Indian Ocean. Path C corresponds to the region lying between Ninetyeast Ridge and the western side of Australia (Table 2). Path D corresponds the region of the wave path crossing the Ninetyeast Ridge, such as earthquakes recorded at SHL and CHG stations (Fig. 1). The inversion of the observed group-velocity data is done using the software package of Herrmann (1987).

Inversion of the Group-Velocity Data

We estimated the mean and standard deviation of the Rayleigh-wave group velocity for the different propagation

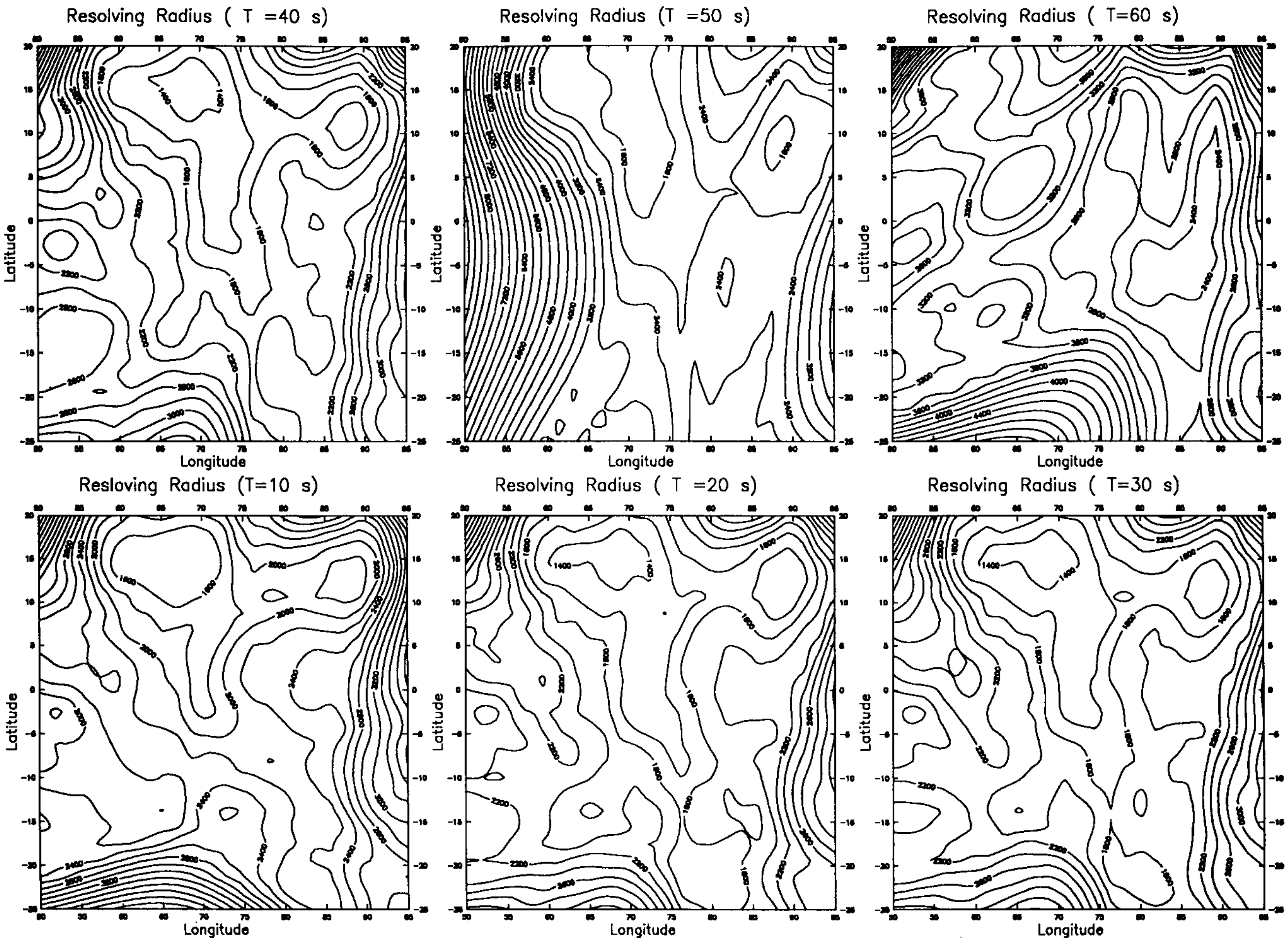

Figure 5. The distribution of the resolving radius of the smoothing area resulted from the inversion of the observed group-velocity data at the periods of 10, 20, 30, 40, 50, and 60 sec.

Table 2

The Propagation Paths between Epicenters and Stations, Divided into Three Groups A, B, and C

Groups	A	B	C
Propagation	1-QUE	1-PRE	1-MUN, PMG
	2-POO, KOD	3-BUL, PRE	2-MUN, PMG
			3-MUN, PMG
Paths	3-NDI, SHI	4-BUL	8-MUN
	7-SHI, NDI	6-AAE	
	8-NDI	7-AAE, NAI	9-MUN, CTA, PMG
		8-BUL, AAE, PRE	12-MUN, PMG
			13-MUN, PMG
		9-BUL, NAI, AAE	14-CTA, PMG, MUN
			15-MUN, PMG
		14-BUL, PRE, NAI	
		16-SLR, NAI	16-MUN

The numbers correspond to the epicenter order as in Table 1.

Table 3
Layer Parameters of Three Initial Models Used in the Inversion with Final Shear-Wave Velocity Models (along with standard deviation)

Layer Thickness (km)	*P* Velocity (km/sec)	*S* Velocity (km/sec)	Density (g/cm^3)	*S* Velocity after Inversion (km/sec) ± S.D.	Thickness after Inversion ± S.D. (km)
Path A					
2.5	1.5	0.0	1.029	0.0	
1.2	4.706	2.5	2.533	2.676 ± 0.05	0.13 ± 1.4
2.0	6.813	3.94	2.738	4.116 ± 0.05	4.90 ± 1.4
15.	8.1	4.15	3.079	4.319 ± 0.05	14.6 ± 1.1
20.	8.2	4.463	3.151	4.309 ± 0.07	23.9 ± 0.4
24.	8.4	4.355	3.6	4.112 ± 0.09	20.0 ± 0.3
20.	8.5	4.35	3.6	4.167 ± 0.09	19.9 ± 0.02
20.	8.7	4.46	3.66	4.357 ± 0.06	19.9 ± 0.1
∝	8.9	4.61	3.76	4.586 ± 0.02	
Path B					
2.5	1.5	0.0	1.029	0.0	
1.2	4.706	2.5	2.533	2.648 ± 0.05	1.04 ± 1.4
2.0	6.813	3.94	2.738	4.088 ± 0.05	1.80 ± 1.0
15.	8.1	4.15	3.079	4.293 ± 0.05	14.5 ± 1.0
20.	8.2	4.463	3.151	4.322 ± 0.07	19.6 ± 0.7
24.	8.4	4.355	3.6	4.122 ± 0.09	23.9 ± 0.3
20.	8.5	4.35	3.6	4.168 ± 0.09	19.9 ± 0.2
20.	8.7	4.46	3.66	4.357 ± 0.06	19.9 ± 0.1
∝	8.9	4.61	3.76	4.588 ± 0.02	
Path C					
2.5	1.5	0.0	1.029	0.0	
1.2	4.706	2.5	2.533	2.648 ± 0.05	1.04 ± 1.4
2.0	6.813	3.94	2.738	4.088 ± 0.05	1.80 ± 1.0
15.	8.1	4.15	3.079	4.293 ± 0.05	14.5 ± 1.0
20.	8.2	4.463	3.151	4.322 ± 0.07	19.6 ± 0.7
24.	8.4	4.355	3.6	4.122 ± 0.09	23.9 ± 0.3
20.	8.5	4.35	3.6	4.168 ± 0.09	19.9 ± 0.2
20.	8.7	4.46	3.66	4.357 ± 0.06	19.9 ± 0.1
∝	8.9	4.61	3.76	4.588 ± 0.02	
Path D (across Ninetyeast Ridge)					
3.5	1.5	0.00	1.029	0.00	2.25
0.85	1.651	0.34	1.029	0.477 ± 0.007	0.17
0.75	2.001	0.81	1.099	0.947 ± 0.007	0.79
0.8	2.303	1.518	1.797	1.665 ± 0.007	2.61
2.2	4.706	2.5	2.533	2.68 ± 0.007	4.07
15.	6.813	3.94	2.738	4.188 ± 0.009	15.1
15.	8.1	4.65	3.079	4.751 ± 0.004	15.1
40.	8.16	4.763	3.051	4.73 ± 0.005	39.9
40.	8.4	4.45	3.06	4.459 ± 0.004	39.9
40.	8.5	4.35	2.26	4.383 ± 0.002	39.9
40.	8.7	4.46	3.31	4.487 ± 0.01	39.9
∝	8.9	4.61	3.36	4.624 ± 0.06	

paths for the selected regions grouped into four different paths, as discussed previously; the details are listed in Table 2 and shown in Figure 1. A simple oceanic model was selected for the initial model and the layer parameters are listed in Table 3. The Herrmann's software (1987) package does the inversion for both the shear-wave velocity and the depth-inversion process. But the depth inversion was done at the final stage, when the match between the observed and the calculated theoretical dispersion curves for the Rayleigh wave seems to be good after the inversion. The inversion was stopped when there was no improvement in the rms error after the iteration of the inversion process. The layer parameters for the final selected velocity models for the four different regions are listed in Table 3 along with the standard deviation in each layer and are shown in Figure 6 for different regions. The calculated and observed dispersion values are shown in Figure 7 for the Rayleigh wave. The standard deviation in most cases (Fig. 7) is more, because the propagation path is complex and numerous heterogeneities are present because of the presence of different lithological boundaries/cracks and fissures, and we had not considered that anisotropy and lateral variations in the layers and inhomogeneity would give rise to more variation in the group-velocity values.

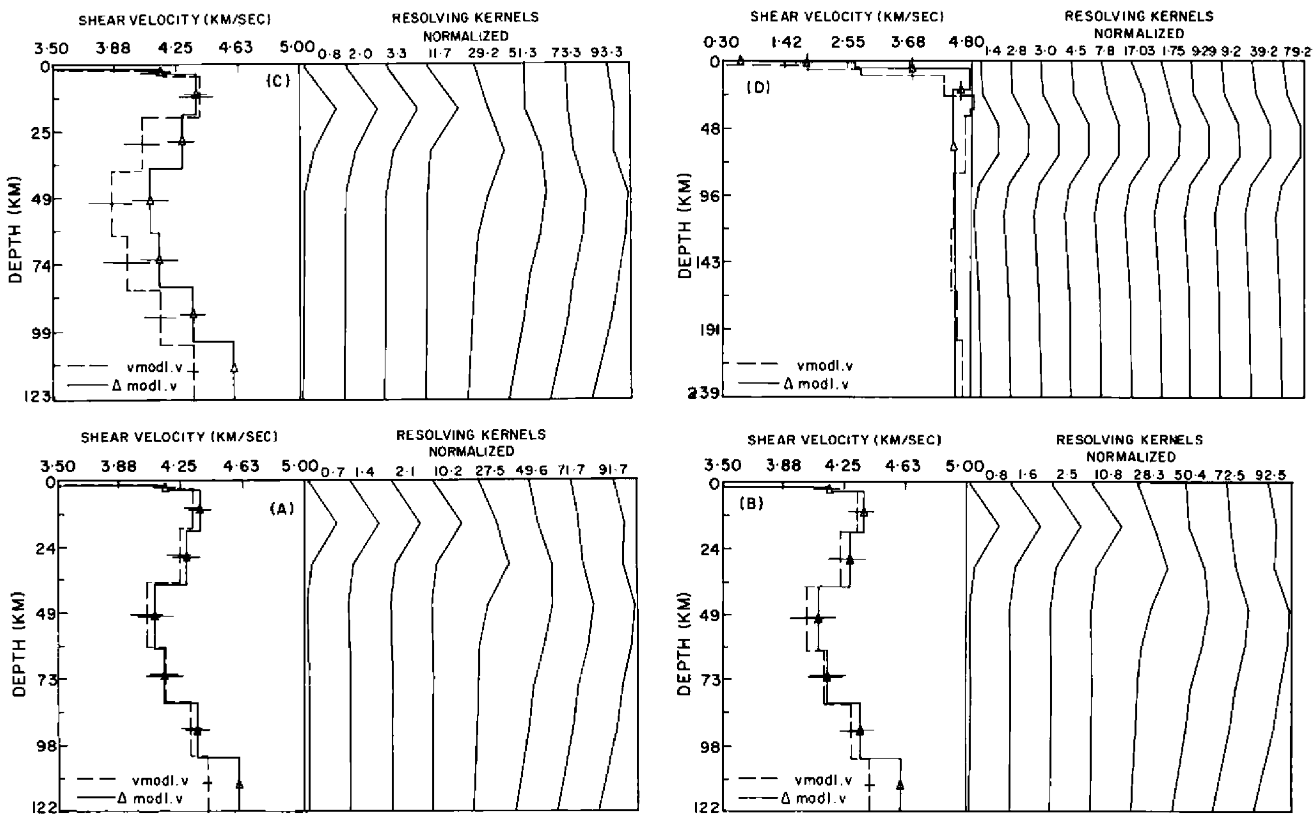

Figure 6. Shear-wave velocity models are shown on the left and result from the inversion of Rayleigh-wave group-velocity data for four different regions traversed by paths in groups of (A) path A; (B) path B; (C) path C; and (D) path D. The right side of the figure shows the resolving kernels for the best-fitting models (left side) for regions traversed by paths in groups A, B, C, and D.

Scatter observed in the group velocity is a reflection of both systematic and random errors. These include errors in the travel time due to source finiteness and rise time. We did not consider these errors, because the earthquakes considered are of small magnitude so that the error term is insignificant.

The best-fit models are shown in Figure 6 for the different propagation paths of the subdivided regions. The resolving kernels are shown in Figure 6 for regions of A, B, C, and D. They do not show good resolution at the deeper depth. In some cases it is good resolution. The resolution is bad for the upper water layer (excluding the top water layer, and this depth has been taken fixed at 2.5-km thickness because the average bathymetry value for the region is 2.5 km). The resolution of the layers that lie above and below Moho is good and the rms error is about 1 km or less.

Results and Discussion

At 10 sec, the isolines of group-velocity (3.3–3.8 km/sec) distribution are gradually decreasing from southern India (3.8 km/sec) to 3.3 km/sec near the northern part of the Bay of Bengal Fan (Fig. 3). For 30 sec and greater the isoline values show higher group velocity (3.9–4.2 km/sec) over the Bay of Bengal. Brune *et al.* (1992) used the data from surface-wave dispersion, seismic refraction, S_N attenuation, and geology and proposed a superthick (~22 km) sedimentary basin under the northern Bay of Bengal, which agrees well with our observed lower group-velocity isolines at 10 sec (Fig. 3). Figure 3 shows high group-velocity isoline values (3.9 to 4.2 km/sec) at 30 to 60 sec over the Bay of Bengal and agrees with the cold upper mantle beneath the region inferred from the high-frequency S_N data (Brune *et al.*, 1992).

Central Indian Basin (10° S, 85° E) shows lower group velocity (2.2 km/sec) at 10 sec for the Rayleigh wave. If we move in the northern direction from the latitude of 25° S across the crest of the isolines of the Rayleigh wave at the 10-sec period along the 90° E longitude, there is a gradual increase in the group-velocity isolines in both the east and west directions (Fig. 3). The present resolution does not permit us to identify seperately the 90° E ridge or 85° E ridge axis, but the combined effects can be seen on the map. As we move in the northern (north-northwest) direction from the Rodriguez triple junction (25° S, 70° E), the group-velocity isolines at the 10-sec period are increasing in the

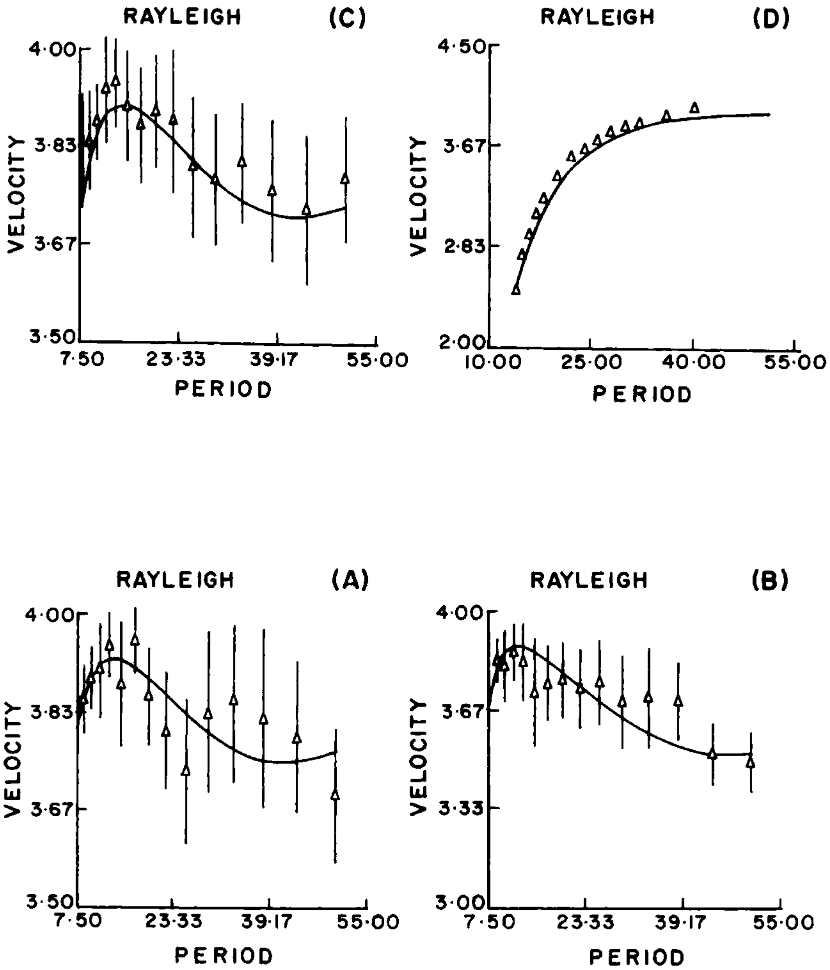

Figure 7. Theoretical and observed group velocities for the best-fitting Rayleigh wave velocity for the regions of (*A*) path A; (B) path B; (C) path C; and (D) path D, respectively. The standard deviation is shown by the vertical bar.

northern direction in both the east and west sides of the ridge axis (Fig. 3) and this agrees with the increase in the age of the ocean floor. These observations can be interpreted as being due to the hot uprising convection current; the material shows low shear-wave velocity along the ridge axis and, farther away from the ridge axis, the material has become cooler with higher shear-wave velocity.

The observed group-velocity isolines for the Rayleigh wave at 10 sec are increasing from 25° S to 10° N latitude along the Ninetyeast Ridge and reach maximum value below north of Sri Lanka (3.8 km/sec at 10 sec to 4.2 km/sec at 50 sec) (Fig. 3). This indicates the presence of lower shear-wave velocity material below the Ninetyeast Ridge at the latitude of 25° S in the depth of 10 km and higher shear-wave velocity at greater depth (≥20 km). The inversion of Rayleigh-wave group-velocity data has shown a 7.5-km-thick crust beneath the Ninetyeast Ridge (Table 3, path D; Fig. 6D) and high shear-wave velocity below Moho (4.19 to 4.75 km/sec). Souriau (1981) has estimated the shear-wave velocity beneath the Ninetyeast Ridge above and below Moho as 3.9–4.27 and 4.5 km/sec and LVZ at 60 km depth from the water surface. In this study, we have estimated higher shear-wave velocity (4.38–4.78 km/sec) of 120 km thickness at 40 km depth from the water surface beneath the Ninetyeast Ridge. This indicates the cold and dense lithosphere beneath the Ninetyeast Ridge. Schlindwein *et al.* (2003) have estimated an approximately 0.16-km-thick layer of pelagic sediments with velocities of 1.5–1.6 km/sec, which is underlain by a layer of volcaniclastic material with 2.2–3.0 km/sec. Velocities rapidly increase from approximately 3.5 to 6.2 km/sec at 5–6 km depth below the seafloor. Grevemeyer *et al.* (2001) have estimated a crustal thickness of 6.5–7.0 km from deep seismic sounding studies, which agrees well with our Moho depth estimates (Table 3). Wide-angle reflections from both the prehotspot and posthotspot crust-mantle boundary suggest the crust under the ridge has been bent downward by loading the lithosphere, and hotspot volcanism has underplated the pre-existing crust with material characterized by seismic velocities intermediate upper mantle rocks (7.5–7.6 km/sec). In total, the crust is up to 24 km thick. The crustal structure is pure oceanic type (Table 3, Fig. 6) in the Indian Ocean. Except for the Ninetyeast Ridge (Fig. 6A, B, C), the LVZ (40–44 km thick) is lying 40 km below water surface with lower shear-wave velocity of 4.12–4.17 km/sec.

Lana and Carbonell (1987) estimated the fundamental-mode Rayleigh-wave group-velocity distribution maps at periods ranging from 15 to 90 sec in the Indian Ocean by means of spherical harmonic expansion of the inverse of group velocity and standard least-square methods. They found high velocity around the Rodriguez triple junction, and our results (Fig. 3) also support higher group velocity at the period of 30 sec and above.

Conclusions

The minima of the isolines of Rayleigh-wave group-velocity (2.0–1.9 km/sec) distribution map at 10 sec lie over the Rodriguez triple junction and the southern part of Ninetyeast Ridge (25° S latitude) and there is an increase in the group-velocity value in the northward direction in accordance with the increase in the age of the oceanic floor. The high shear-wave velocity below the Moho depth (4.19–4.75 km/sec) beneath the Ninetyeast Ridge indicates the presence of cold and dense lithosphere. The shear-wave velocity structure beneath the Ninetyeast Ridge shows the crust-upper mantle transition situated at 22.5 km depth, which may be due to the magmatic underplating.

Acknowledgments

I am grateful to Dr. T. B. Yanovskaya, Institute of Physics, Leningrad State University, Leningrad, Russia for her computer program of the surface-wave tomography studies and Prof. R. Herrmann of Saint Louis University, St. Louis, Missouri, for his software package of surface-wave inversion. The valuable suggestions made by Prof. L. R. Dorman helped in improving the manuscript and his contribution of providing Figure 2 is gratefully acknowledged. The research was supported by the Department of Science and Technology, New Delhi, India. I thank Dr. V. P. Dimri, Director, National Geophysical Research Institute, Hyderabad – 5000007 (A.P.), India, for giving the permission to publish the work.

References

Brune, J. N., and D. D. Singh (1986). Continent-like crustal thickness beneath the Bay of Bengal sediments, *Bull. Seism. Soc. Am.* **76,** 191–203.

Brune, J. N., J. Curray, L. R. Dorman, and R. Raitt (1992). A proposed super-thick sedimentary basin, Bay of Bengal, *Geophys. Res. Lett.* **19,** 565–568.

Dziewonski, A., S. Bloch, and M. Landisman (1969). A technique for the analysis of transient seismic signals, *Bull. Seism. Soc. Am.* **59,** 129–139.

Gobarenko, V. S., S. B. Nikolova, and T. B. Yanovskaya (1987). 2-D and 3-D velocity patterns in southeastern Europe, Asia Minor and the eastern Mediterranean from seismological data, *Geophys. J. R. Astr. Soc.* **90,** 473–484.

Grevemeyer, I., E. R. Flueh, C. Reichert, J. Bialas, D. Klaschen, and C. Kopp (2001). Crustal architecture and deep structure of the Ninetyeast Ridge hotspot trail from active-source ocean bottom seismology, *Geophys. J. Int.* **144,** 414–431.

Herrmann, R. B. (1987). Computer programs in Seismology, User's Manual, Vol. **IV,** St. Louis University, St. Louis, Missouri.

Lana, X., and R. Carbonell (1987). Surface harmonic expansion methodology in restricted domains of the Earth's surface. Application to the Indian Ocean, *J. Geophys.* **61,** 158–167.

Montagner, J. P. (1986). 3-dimensional structure of the Indian Ocean inferred from long period surface waves, *Geophys. Res. Lett.* **13,** 315–318.

Montagner, J. P., and N. Jobert (1988). Vectorial tomography, II. Application to the Indian Ocean, *Geophys. J. Int.* **94,** 309–344.

Patnaik, G. B., and B. J. Mitchell (1984). Lateral variation of shear-wave velocities in the Eastern Indian Ocean from seismic surface waves (abstract), *EOS Trans. AGU* **65,** 245.

Roult, G., G. Rouland, and J. P. Montagner (1987). Phase velocity distribution in the Indian Ocean and Indonesian region inferred from geoscope records, *Geophys. Res. Lett.* **14,** 343–346.

Schlindwein, V., C. Bonnemann, C. Reichert, I. Grevemeyer, and E. Flueh (2003). Three-dimensional seismic refraction tomography of the crustal structure at the ION site on the Ninetyeast Ridge, Indian Ocean, *Geophys. J. Int.* **152,** 171–184.

Singh, D. D. (1988a). Quasi-continental oceanic structure beneath the Arabian Fan sediments from the observed surface wave dispersion studies, *Bull. Seism. Soc. Am.* **78,** 1510–1521.

Singh, D. D. (1988b). Crust and upper mantle velocity beneath north and central Indian Ocean from the phase and group velocity of Rayleigh and Love waves, *Phys. Earth Planet. Interiors* **50,** 230–239.

Souriau, A. (1981). The upper mantle beneath Ninetyeast Ridge and Broken Ridge, Indian Ocean, from surface waves, *Geophys. J. R. Astr. Soc.* **67,** 359–374.

Teng, T. L., and A. Ben-Menahem (1965). Mechanism of deep earthquakes from spectrums of isolated body wave signals, *J. Geophys. Res.* **70,** 5157–5170.

Wu, F. T., and A. Levshin (1994). Surface wave group velocity tomography of East Asia, *Phys. Earth Planet. Interiors* **84,** 59–77.

Yanovskaya, T. B. (1982). Group velocity distribution of surface waves in the north Atlantic, Izvestiya, *Phys. Solid Earth* **18,** 83–89.

National Geophysical Research Institute
Hyderabad – 500007 (A.P.) India

Manuscript received 12 December 2000.